Materials Science and Engineering C 39 (2014) 92–99

Contents lists available at ScienceDirect

Materials Science and Engineering C

journal homepage: www.elsevier.com/locate/msec

A low detection limit penicillin biosensor based on single graphene nanosheets preadsorbed with hematein/ionic liquids/penicillinase

Yueting Wu [a,b,c], Lele Tang [a,b,c], Linhong Huang [a,b,c], Zhizhong Han [b,c], Jian Wang [c], Haibo Pan [a,b,c,*]

[a] Fujian Key Lab of Medical Instrument & Pharmaceutical Technology, Yishan Campus, Fuzhou University, Fuzhou, Fujian 350002, China
[b] Institute of Research for Functional Materials, Yishan Campus, Fuzhou University, Fuzhou, Fujian 350002, China
[c] College of Chemistry and Chemical Engineering, Qishan Campus, Fuzhou University, Fuzhou, Fujian 350108, China

ARTICLE INFO

Article history:
Received 29 September 2013
Received in revised form 21 January 2014
Accepted 8 February 2014
Available online 17 February 2014

Keywords:
Penicillin biosensor
Electrochemistry
Graphene nanosheets
Ionic liquids
Hematein

ABSTRACT

In this study, we reported on a low detection limit penicillin biosensor with layer-by-layer (LbL) film containing single-graphene nanosheets (SGNs) preadsorbed with hematein, ionic liquids (ILs) and penicillinase. The penicillinase catalyzes the hydrolysis of penicillin to penicilloic acid, where H^+ is liberated and monitored amperometrically with hematein as a pH indicator. The SGN-hematein/ILs/penicillinase biosensor exhibited excellent performance for penicillin in PBS with a wide range from 1.25×10^{-13} to 7.5×10^{-3} M, and a low detection limit of 10^{-13} M (0.04 ppt, S/N ≥ 3). Furthermore, the detection of penicillin concentration in real sample (milk) had acceptable accuracy with the assay system.

1. Introduction

Penicillin is a highly effective β-lactam antibiotic based on a β-lactam ring which is responsible for the antibacterial activity, and has variable side chains due to their chemical and pharmacological properties. Therefore, it is widely applied to prevent and treat various bacterial infections in human and livestock [1], and even added to feedstuff to promote animal growth [2,3]. The presence of antibiotic residues in food products, drinking water, and environment constitutes a worldwide concern because of its serious health consequences, including the emergence of antibiotic-resistant bacterial strains, disturbance or disruption of the normal ecological equilibrium, and increasing instances of allergic reactions. Penicillins and other lactam antibiotics are the most frequently used antibiotics and have long been widely used for treating various bacterial infections in human, livestock, poultry, and aquaculture. The presence of penicillin residues represents a potential hazard to public health, since they can cause the formation of antibiotic-resistant bacterial strains and allergic reactions [2]. Approximately 5–10% of the population is hypersensitive to penicillin or other antibiotics, and suffers allergic reactions at concentrations as low as 1 ppb ($\approx 2.8 \times 10-^9$ M) penicillin [4].

To date, various analytical methods have been reported for the determination of penicillin residues, including capillary electrophoresis (CE) [5], high-performance liquid chromatography (HPLC) [6], liquid chromatograph-mass spectrometer (LC-MS) [7], liquid chromatography–electrospray ionization mass spectrometry (LC-ESI/MS) [2], pressurized liquid extraction and high-performance liquid chromatography with ultraviolet detection (PLE-HPLC-UV) [8] and immunosorbent assays [9–11]. Although the determination of penicillin residues by these methods is reliable and quite sensitive, these instruments are inherently expensive. And also the pretreatment for samples involved as well as these operating processes are complicated and longer. Consequently, it is crucial to develop a simple, rapid and sensitive analysis method for the determination of penicillin residues in food and environmental monitor.

Electroanalysis is an appropriate route for detection of penicillin residues, because penicillinase can catalyze the hydrolysis of penicillin to penicillinic acid, resulting in a decrease of solution pH. Recently, various penicillin sensors have been reported based on the measurement of the change of pH with potentiometric [12,13] and capacitive [14,15] technique, respectively. But they still have a drawback of complex in configurations and relatively high detection limits (0.005–0.5 mM) [12–15]. Another way to simplify the fabrication and improve the detection limit is used by amperometric technique for penicillin biosensors [1,16]. Bi et al. devised an amperometric biosensor for detecting penicillin residues by using hematein as a pH-sensitive redox probe, multi-walled carbon nanotubes (MWCNT) as an electron transfer enhancer, and chitosan as a film-forming polyelectrolyte. The amperometric biosensor has many

* Corresponding author at: College of Chemistry and Chemical Engineering, Qishan Campus, Fuzhou University, Fuzhou, Fujian 350108, China. Tel.: +86 591 83759450/22866339; fax: +86 591 22866127.
E-mail address: hbpan@fzu.edu.cn (H. Pan).

http://dx.doi.org/10.1016/j.msec.2014.02.012
0928-4931/

advantages over conventional sensors, such as potentiometric, conductometric, and capacitive sensors, in terms of higher sensitivity, lower detection limit (50 nM), shorter response time, simplicity and lower cost [1].

As known, graphene, an emerging true two-dimensional carbon nanomaterial [17,18], is a monolayer of sp^2-bonded carbon atoms densely packed into a honeycomb crystal structure [19]. Compared to single wall carbon nanotubes (SWCNTs), the single-graphene nanosheets (SGNs) exhibit 60 times more conductivity [19], larger surface area [20], better sensitivity and stability as well as greater sp^2 character [21]. Thus, researches on the graphene-based biosensors are fascinating and increasing for sensing biomolecules like glucose [21], NADH [22], dopamine [23], etc. Besides, ionic liquids (ILs), composed of a bulky organic cation and either an organic or an inorganic anion, have attracted more and more attention in electrochemical biosensors due to its intrinsic properties, such as wide electrochemical window, well biocompatibility, good film stability and high ionic conductivity for the enhanced electrochemical response [24–26]. Maleki et al. developed an ionic liquid modified carbon paste electrode with 1-octylpyridinium hexafluorophosphate (OPFP) as binder and further used it for the detection of some electroactive molecules [27]. It is found that the mixture or combining of graphene and ILs could improve their conductivity, compatibility and stability, inducing more applications of graphene in the electrochemical field [28–30].

In the work, we investigated the performance of modified electrodes with layer-by-layer (LbL) films containing single-graphene nanosheets preadsorbed with hematein (SGN-hematein), ILs and penicillinase for the determination of penicillin residues by employing cyclic voltammetric (CV) and differential pulse voltammetry (DPV). Herein, the SGNs were synthesized by the reducing of graphene oxide with $NaBH_4$ [31]. The surface morphologies and properties of the SGNs samples were researched by UV–VIS, XRD, HRTEM, AFM and electrochemical measurements. In addition, the ILs play an important role in the film-forming, high ionic conductivity and immobilization with negatively charged penicillinase via electrostatic attractions. The resulted SGN–hematein/ILs/penicillinase biosensor is successfully applied to the voltammetric determination of penicillin with high sensitivity. The system was employed to analyze penicillin in milk samples that included penicillin. Finally, the performance features such as reproducibility, stability and specificity were evaluated.

2. Experimental

2.1. Materials

Graphite powder (99.95%, 325 mesh) was obtained from Alfa Aesar (Tianjin, China). Penicillin G sodium salt was purchased from Aladdin Chemistry Co. Ltd (Shanghai, China). Penicillinase (1 ml will inactivate 120,000 units of Penicillin stored at 4 °C) and hematein were provided by J&K Scientific Ltd. (Shanghai, China). The ionic liquids, trihexyltetradecylphosphonium bis (trifluoromethylsulfonyl) imide ($[P(C_6)_3C_{14}][Tf_2N]$, purity: 98%), were supplied by Sigma-Aldrich and used as received. The phosphate buffer solution (PBS) was prepared using K_2HPO_4 and KH_2PO_4. The penicillin G solutions and penicillinase solutions were prepared with 1 mM pH 7.0 PBS (containing 0.1 M NaCl) in all experiments. All other chemicals used were of analytical reagent grade. Ultra-pure water was obtained with a Milli-Q plus water purification system (Millipore Co. Ltd., USA) (18 MΩ). Milk samples, containing protein ≥2.9% (w/w) and fat ≥3.3% (w/w), were purchased from a local supermarket. The spiked milk samples were filtrated by a hollow fiber membrane module to remove protein and fat, and then the supernatants were collected as real sample in PBS.

2.2. Apparatus

UV–VIS measurements were conducted at a UV-1800 SHIMADZU UV–VIS spectrophotometer (SHIMADZU, Japan). High-resolution transmission electron microscope (HRTEM) image was obtained using Tecnai G2 F20 S-TWIN, 200 kV (FEI Company, USA). The samples were prepared by diluting a few milliliters of the SGN suspension with ethanol, followed by pipetting a few microliters onto a copper grid, and then dried under ambient temperature. Atomic force microscopy (AFM) images were recorded using a Nanoscope IIIa multimode atomic force microscope (Veeco Instruments, USA) in tapping mode to simultaneously collect height and morphology data. A droplet of SGN dispersion (about 0.01 mg mL^{-1}) was casted onto a freshly cleaved mica surface, then dried in N_2. X-ray diffraction (XRD) measurements of the samples were recorded on a Rigaku-miniflex X-ray powder diffractometer using Cu Kα radiation ($\lambda = 1.5306$ A) with scattering angles (2θ) of 5–80°. Zeta-potential value measurement of the samples was performed on Zeta Sizer3000 Laser Particle Size and Zeta Potential Tester (Malvern Corporation, UK) in aqueous solution.

The electrochemical properties of as-prepared electrodes were characterized by cyclic voltammetric (CV), electrochemical impedance spectroscopy (EIS) and differential pulse voltammetric (DPV). The electrochemical measurements were performed with a three-electrode configuration on a CHI 660D electrochemical workstation (CH Instrument Company, Shanghai, China). The working electrode was a modified glassy carbon electrode (i.e., the SGN-hematein/ILs/penicillinase electrode), and counter electrode and reference electrodes were a platinum wire and a KCl saturated Ag/AgCl electrode, respectively. In biosensing measurements, the CV and DPV measurements of the penicillinase electrode were proceeded in a corresponding PBS solution by applying voltage in the range between −0.4 and 0.8 V versus Ag/AgCl. The resulted current changes were correlated to the final concentrations of penicillin G in the tested solution. The EIS measurements of the penicillinase electrode were recorded at a formal potential of 237 mV (vs. Ag/AgCl) within the frequency range of 1Hz–100 kHz. 5 mV amplitude of sine voltage signal was applied to the three-electrode system under open circuit potential and the number of data points per frequency decade was 12. During the analysis of real sample, the amperometric response of the penicillinase electrode was monitored at 0.2 V in a 20 mL-static electrochemical cell containing 10 mL of 1 mM pH 7.0 PBS-0.1 M NaCl as the supporting electrolyte solution. Aliquots of 1–10 μL of penicillin G spiked in PBS and milk sample solutions were successively injected into the electrochemical cell under magnetic stirring. The resulted current changes were correlated to the final concentrations of penicillin G in the tested solution. All measurements were performed at room temperature.

2.3. Synthesis of graphene

Graphene oxide (GO) was prepared by a modified Hummer's method, graphite powder as raw materials [32]. Then, the as-purified GO suspensions were dispersed in water to yield a yellow–brown dispersion (0.05 wt.%) by ultrasonication for 1 h, following that the dispersion was centrifuged at 8000 rpm for 15 min to remove unexfoliated GO (usually presented in a very small amount). Subsequently, a $NaBH_4$ solution (1 M, 15 mL) was added to GO (75 mL) suspensions under stirring. A 10 wt.% sodium carbonate (Na_2CO_3) solution was used as an acidity regulator to adjust the pH to around 10. After being vigorously shaken or stirred for a few minutes, the vial was put in an oil bath (90 °C) for 1 h. The stable black dispersion was then obtained. The mixture was then allowed to cool at room temperature and filtered with a nylon membrane (0.22 μm) to obtain SGNs. Finally, the resulted-SGNs redispersed readily in water by ultrasonication.

2.4. Preparation of the amperometric penicillin biosensor

Prior to preparation of biosensor, the glassy carbon electrode (GCE) with a diameter of 3 mm was polished on a polished cloth with 0.3 and 0.05 μm alumina powder, respectively. Then the GCE was rinsed with deionized water, ultrasonicated in deionized water and ethanol bath,

respectively. Finally, the GCE was dried at room temperature. The amperometric penicillin biosensor has been prepared by LbL technique. Briefly, 100 μL 0.05 wt.% SGN aqueous dispersion and 100 μL 50 mM hematein aqueous dispersion were mixed, and 5 μL mixture was dropped on the GCE surface. A beaker was covered over the electrode assuring slow evaporation of water and formation of a uniform film but out of pollution. After drying, the electrode was rinsed with 1 mM pH 7.0 PBS to remove unimmobilized SGNs and unadsorbed hematein molecules. 5 μL 10% ILs aqueous dispersion was deposited on the layer of immobilized SGNs preadsorbed with hematein. Then dried again, the electrode was rinsed with 1 mM pH 7.0 PBS. Further, 10 μL of 60,000 U mL^{-1} penicillinase solution was immobilized on SGN-hematein/ILs/GCE and moved into a refrigerator. After being kept at 4 °C overnight, the resulted enzyme electrode was rinsed with 1 mM pH 7.0 PBS to remove unbound enzyme molecules and stored at 4 °C until use.

3. Results and discussion

3.1. Assembly of SGN-hematein/ILs/penicillinase biosensor

Scheme 1 illustrates a representation of the LbL setup for the SGN-hematein/ILs/penicillinase biosensor and its operation principle. As shown, a negatively charged layer of carboxylated SGNs preadsorbed with hematein was casted on GCE through solvent evaporation. Then ILs were dropped on the SGN–hematein/GCE due to its excellent film-forming ability and good biocompatibility which is much favorable to further immobilization of biomolecules [32]. In addition, the penicillinase with an isoelectric point of 5.4 [1] is negatively charged in pH 7.0 PBS. Therefore, the penicillinase is successively assembled onto the layer of SGN-hematein/ILs via electrostatic attraction. The operation principle based on SGN-hematein/ILs/penicillinase biosensor is that the immobilized penicillinase catalyzes the hydrolysis of penicillin into penicilloic acid, and then H^+ is liberated from the penicilloic acid, which causes a decrease in local pH. Once hydrogen ion is accepted, hematein as a pH-sensitive redox probe is reduced to hematoxylin [33], which can cause the signal changing of electrochemical detection. And also, the signal change is proportional to the concentration of penicillin presenting in the sample.

3.2. Characterization of GO and SGNs

The formation of GO and SGN suspension was firstly confirmed by XRD patterns. Compared with the graphite, a sharp diffraction peak of graphite at 26.4° (Fig. 1(a)) disappears and the feature diffraction peak of graphene oxide exists at 10.6° in the XRD pattern of GO (Fig. 1(b)) due to the presence of oxygen-containing functional groups attached on both sides of the GO sheet [34]. After reduction, the obtained SGNs show a broadened diffraction peak at 24.5° (Fig. 1(c)), indicating that the layers of graphite along the c-axis are exfoliated and the carbon sp^2 bonds are restored [20]. This is consistent with the analysis of UV–VIS spectroscopy (Fig. 2). The GO suspension displays two characteristic peaks, i.e., one at 230 nm corresponding to π → π* transition of aromatic C – C bonds, and a shoulder peak at ~300 nm to n → π* transitions of C═O bonds [35]. While the SGN suspension exhibits a bathochromic shift of the absorption peak (230 nm) to 270 nm after the chemical reduction treatment, suggesting that the restoration of π-conjugated network within the graphene sheets occurs upon chemical reduction [36,37]. The inset in Fig. 2 is the photographic images of GO suspension (yellow–brown) and SGN suspension (black) preserved in the centrifugal tube with plug after depositing for ten months. The color of the samples is not changed noticeably and they still well disperse in aqueous phase without any agglomerate deposition, indicating that the GO and SGN dispersions are very stable due to the presence of the carboxylic acid groups on the SGN surface.

In Fig. S1, our study on the surface charge (zeta potential) of as-prepared SGNs displays that these sheets hold a negative charge of −34.3 mV in water. Meanwhile, based on FT-IR spectra of GO and SGNs (Fig. S2), the increased absorption band at around 1500 cm^{-1} in

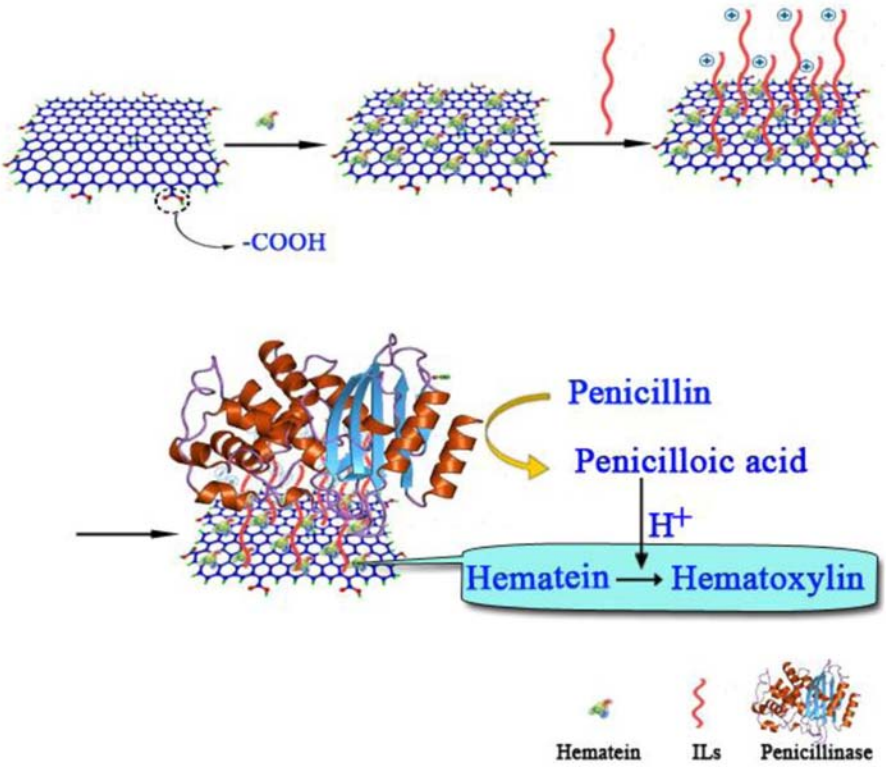

Scheme 1. A representation of the LbL setup for SGN-hematein/ILs/penicillinase biosensor and its operation principle.

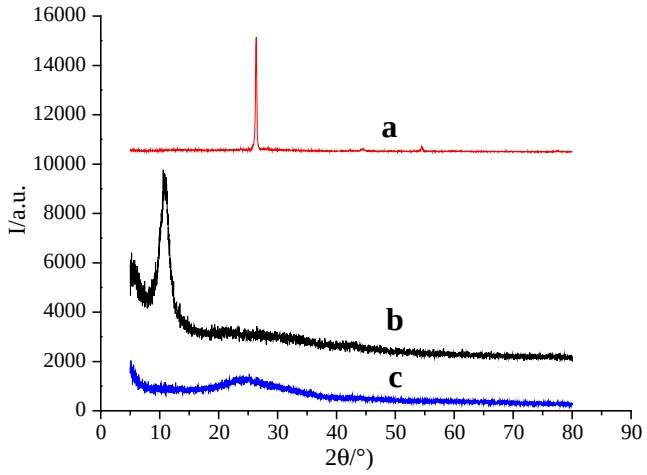

Fig. 1. XRD patterns of (a) graphite, (b) GO and (c) SGNs.

SGNs can be obviously noticed, which is attributed to the skeletal vibration of graphene sheets. A weaker one at ~1725 cm^{-1} still remained in SGNs, which is attributed to carboxyl groups. Also it could be seen that the vibrational bands of oxygen-containing groups at 1060, 1230, 1629 and 3440 cm^{-1} disappeared in the spectrum of SGNs, indicating that GO has been reduced to SGNs completely. Based on the zeta potential and FTIR results, we could conclude that the surface of the SGNs is negatively charged as a result of ionization of the carboxylic acid groups. It suggests that the formation of stable SGN aqueous solution should be attributed to electrostatic repulsion due to the presence of carboxylic acid groups.

To further confirm the detailed morphological of the SGN sample, HRTEM photographs were taken in different magnifications (Fig. 3A and B). A large graphene nanosheet (a few hundred square nanometers) is observed to situate on the top of the copper grid in Fig. 3A. Meanwhile, a perfect graphene nanosheet is clearly distinguished in the HRTEM image (Fig. 3B). The SGNs are not perfectly flat [36] but rippled, indicating that the SGNs have the features of high surface/volume ratio and two-dimensional structure [29].

AFM characterization is the most direct method of quantifying the thickness of samples. The AFM images reveal the presence of irregularly shaped SGNs with uniform thickness and lateral dimensions ranging from a few hundred nanometers to a few micrometers in Fig. 3C. The height profile diagram shown in the thickness of the SGN is typically between 0.7 and 0.9 nm, corresponding with the thickness of a single graphene nanosheet in the early literature [38]. The graphene nanosheets are thicker than that of the theoretical thickness of a single graphene layer (0.34 nm) due to the existence of carboxylic acid groups. As expected, the AFM investigations illuminate that the individual GNs were fully exfoliated in water. And also, these SNGs could be steadily suspended in aqueous solution even for over ten months as the inset of Fig. 2.

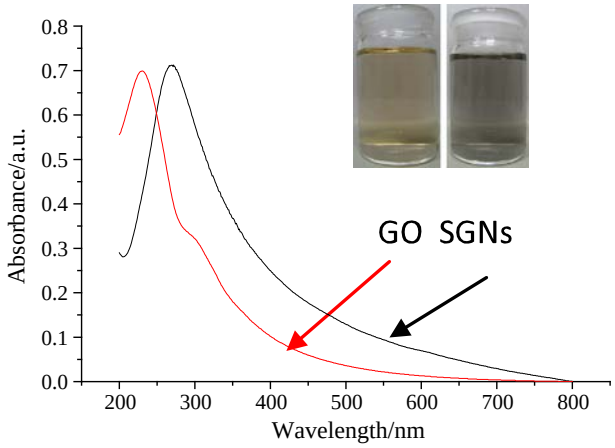

Fig. 2. UV–Vis spectra of GO (yellow–brown) and SGNs (black). Inset is the photographic images of GO and SGNs.

3.3. Electrochemical properties of SGN-hematein/ILs/penicillinase electrode

Fig. 4 displays typical cyclic voltammograms (CVs) of penicillinase/GCE (a), SGNs/ILs/GCE (b), hematein/GCE (c) and SGN-hematein/GCE (d) in the PBS over a potential ranging from −0.2 V to 0.8 V at a scan rate of 0.1 V s^{-1}. No oxidation or reduction process appears at penicillinase/GCE (a) and SGNs/ILs/GCE (b), indicating that penicillinase, SGNs and ILs are not electroactive within this potential range. For the C–V curve (Fig. 4(c)), there is a couple of nearly reversible and well-defined redox peaks with small current. The separation of cathodic and anodic peak potential amounts to ~60 mV, and the ratio of oxidation and reduction peak currents approximates to 1, representing that the characteristics of the reversible electron transfer occurs between hematein and hematoxylin (inset of Fig. 4) [39]. Furthermore, after hematein was mixed with SGNs and then assembled on GCE, the CV current of SGN-hematein/GCE (Fig. 4(d)) is larger than that of hematein/GCE (Fig. 4(c)). It is obvious that the SGNs play a crucial role in providing large surface area for loading hematein and facilitating electron transfer between hematein and GCE.

Among the various transduction techniques, electrochemical impedance spectroscopy (EIS) is a highly effective method ($Z*(\omega) = Z'(\omega) + j\cdot Z''(\omega)$, the angular frequency $\omega = 2\pi f$, where f is frequency) to probe the interfacial properties and confirm the assembly of the modified electrode in this work [40]. By using the solution-based redox probe $[Fe(CN)_6]^{3-/4-}$, the Nyquist plots of different modified electrodes are shown in Fig. 5, where the semicircle portions at high-frequency correspond to the electron transfer resistance at the electrode surface and the straight lines at the low frequency correspond to the diffusion of a redox couple. Due to high resistance for penicillinase, the electrochemical impedance for modified electrode greatly increases after penicillinase was modified onto SGN-hematein modified electrode. As seen in Fig. 5, the sequence of the values of charge-transfer resistance (R_{ct}) for different electrodes in this work is SGN-hematein/penicillinase/GCE (curve c) > SGN-hematein/ILs/penicillinase/GCE (curve d) > SGN-hematein (curve b) > bare GCE (curve a). Obviously, the electronic transport at the SGN-hematein/ILs/penicillinase/GCE is faster than that of SGN-hematein/penicillinase/GCE due to the existence of ILs with high ionic conductivity in the modified films.

Fig. S3 depicts the CVs of the SGN-hematein/ILs/penicillinase/GCE at various scan rates and the plots of peak currents versus scan rate. The reduction and oxidation currents increase linearly with the scan rate, demonstrating that the electrochemical reaction of hematein on SGN-hematein/ILs/penicillinase/GCE is a quasi-reversible surface-controlled process.

3.4. pH Effect for the SGN-hematein/ILs/penicillinase/GCE biosensor

The influences of pH on the reduction peak current and peak potential of the SGN-hematein/ILs/penicillinase/GCE were investigated in the pH range of 7 to 4 using 1 mM PBS applying differential pulse voltammetric (DPV). It can be seen that the reduction peak current is significantly affected by changing the pH of the supporting electrolyte to an acidic range (Fig. 6). As the pH value decreases, the reduction peak of SGN-hematein/ILs/penicillinase/GCE sharply increases. Due to the lowest peak current at pH 7.0, the pH value was chosen for the present analytical applications. In addition, the reduction peak shifts to more positive values by decreasing the pH in the supporting electrolyte. At a lower pH, the cathodic peaks of hematein appear to separate into two peaks, which may be attributed to the redox reaction of hematein involved in a two-electron electrode process (inset of Fig. 6).

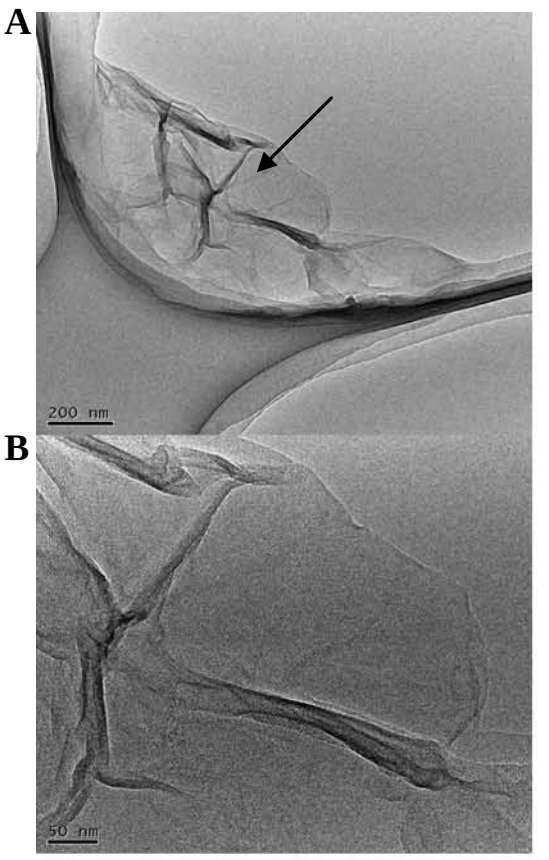

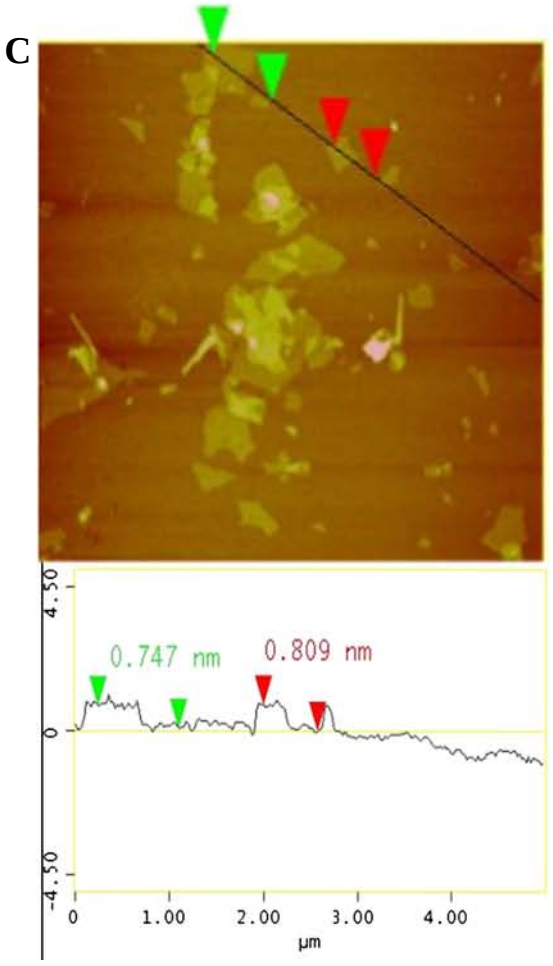

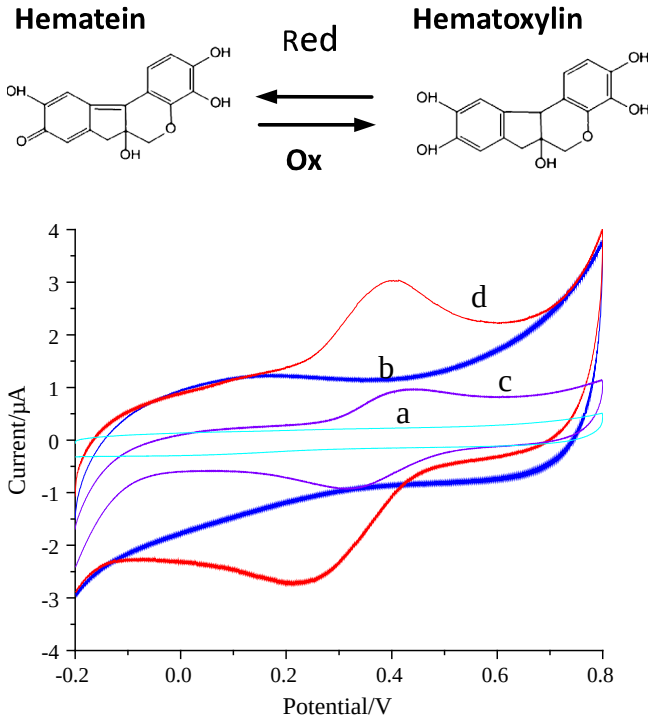

Fig. 4. Cyclic voltammograms of (a) penicillinase, (b) SGNs/ILs, (c) hematein and (d) SGN-hematein modified electrodes in 1 mM pH 6.8 PBS solution at a scan rate of 0.1 V s^{-1}. Inset is the oxidation and reduction of hematein–hematoxylin.

3.5. DPV investigation and calibration characteristics of SGN-hematein/ILs/penicillinase/GCE

The electrochemical behaviors of SGN–hematein/ILs/penicillinase/GCE changed with the addition of penicillin G are further studied in DPV mode in 1 mM pH 7.0 PBS solution (containing 0.1 M KCl). As to the increase of reduction current after the addition of penicillin to the cell, it may be due to the hydrolysis of penicillin into penicilloic acid by penicillinase catalyzing. Then H^+ was liberated from the penicilloic acid. Once hydrogen ion is accepted, hematein as a pH-sensitive redox probe is reduced to hematoxylin, and it induces the signal increase of electrochemical detection. As an evidence from Fig. 7A, the reduction peak current at 0.2 V increases with the addition of penicillin G. Three linear regression lines of penicillin G concentration versus cathodic peak current of DPV are presented in Fig. 7B and C. For clarity, the response of DPV peak current increases with increasing the analyte concentration from 1.25×10^{-13} M to 7.5 mM (0.05 ppt to 2.67×10^3 ppm) and reaches a plateau thereafter. From 1.25×10^{-13} M to 1 μM (0.05 ppt to 1 ppb) (Range I), the response is linearly correlated to the logarithmic concentration of penicillin G (Fig. 7B). Following two linear regions are plotted in the ranges of 1 μM to 3.11 mM (1 ppb to 1.11×10^3 ppm) (Range II) and 3.11–7.5 mM (1.11×10^3–2.67×10^3 ppm) (Range III) (Fig. 7C). The corresponding linear functions are $I_{pc}/\mu A = 1.30(\pm 0.03) + 0.16\lg([PEN]/\mu M)$ ($R^2 = 0.996$), $I_{pc}/\mu A = 1.22(\pm 0.03) + 0.81([PEN]/mM)$ ($R^2 = 0.998$) and $I_{pc}/\mu A = 3.17(\pm 0.04) + 0.18([PEN]/mM)$ ($R^2 = 0.995$), where [PEN] is the concentration of penicillin G. With the criterion of S/N ≥ 3 and noise of baseline (0.05967 μA), the ultra-low limit of detection was measured to be 10^{-13} M (0.04 ppt) from Fig. 7B. This could be explained by the fact that the activity of the immobilized penicillinase can be inhibited by the acidic products of the enzymatic hydrolysis when the acidic products were accumulated to a certain high level.

Fig. 3. TEM images of SGNs (A: low magnification and B: high magnification at arrow part of A), (C) AFM image of SGNs and a thickness profile of SGNs marked by the black line.

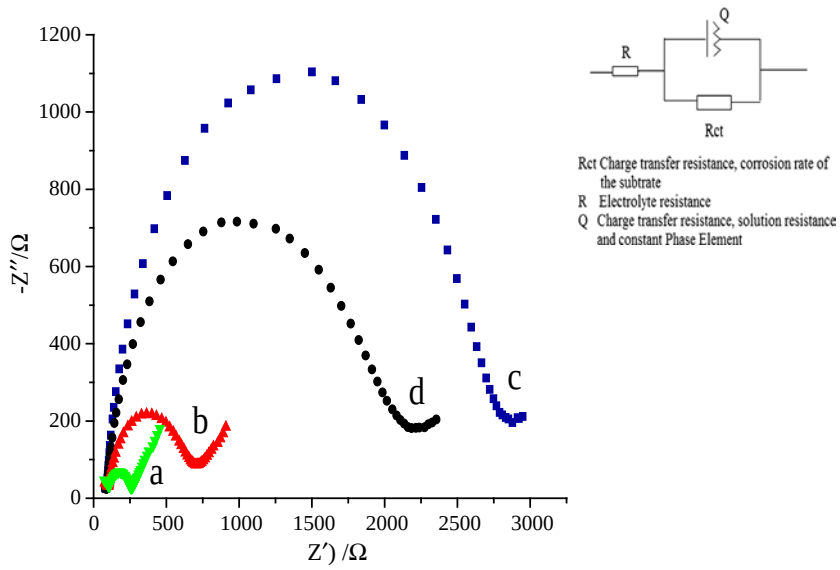

Fig. 5. Electrochemical impedance spectroscopies for (a) bare GCE, (b)SGN-hematein/GCE, (c) SGN-hematein/penicillinase/GCE and (d) SGN-hematein/ILs/penicillinase/GCE in a solution of 5.0 mM $K_4Fe(CN)^{3-}{}_6/K_3Fe(CN)^{4-}{}_6$ + 0.1 M KCl. (Inset: an equivalent circuit).

Within the low concentration range (Range I), the influence of the inhibition effect is negligible. While at the higher concentration of penicillin G (Ranges II and III), the enzyme activity is lowered due to accumulation of the acidic products, inducing that the system becomes less sensitive [1].

We have summarized various analytical methods for penicillin G in Table 1 with respect to the linear range and the detection limit. It can be seen that the performance of this developed sensor is better than other penicillin sensors in the references.

3.6. Analysis of milk sample

To further assess the possible application of our proposed sensor for real sample analysis, the concentration of penicillin in milk solution was determined. The milk for detection was bought from a supermarket in China, and then, the macromolecules over 6000 were removed by a hollow fiber membrane (LX-UF-200 × 1524-3 × 6000-PS, Tianjing Mozhongmo Tech. Co., China). Three contents of penicillin, 10.00, 50.00 and 100.00 nM, were injected into 1 mM PBS, respectively. Finally, the standard addition method was used to determine the average recovery of penicillin. Table S1 summarizes the results of the SGN-hematein/ILs/penicillinase biosensor for detecting penicillin G spiked in milk at a working potential of 0.2 V. For the milk samples, relative standard deviations (RSD) were less than 4.5% and detection limit was 10^{-9} M. Thus the SGN-hematein/ILs/penicillinase biosensor can be successfully used for determination of penicillin residues in milk.

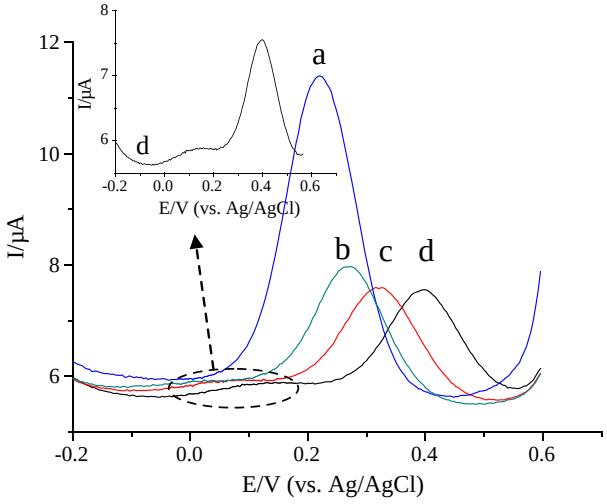

Fig. 6. Differential pulse voltammetric response (DPV) of the SGN-hematein/ILs/penicillinase electrode in 1 mM PBS with different pH values: (a) pH 7, (b) pH 6, (c) pH 5 and (d) pH 4.

3.7. Reproducibility, stability and selectivity

The cyclic voltammetric responses of the SGN-hematein/ILs/penicillinase electrode in the presence of 1nM penicillin G PBS solution represent no obvious change after 20 cycles, and the RSD of the current response to 1 nM penicillin G at 0.2 V is 3.1%, indicating that the GN-hematein/ILs/penicillinase electrode is stable. The storage stability of the modified electrode is further investigated. The cathodic peak currents are measured using the same electrode and still retain above 95% of its initial response stored at 4 °C after 3 days and maintain 80% after 1 week. These results display that the direct electrochemistry of hematein at the SGN-hematein/ILs/penicillinase electrode has a good stability and reproducibility.

The selectivity of the present biosensor was investigated by comparing its responses to penicillin G, another β-lactam antibiotic (ampicillin sodium salt), and three non-β-lactam antibiotics (namely Kanamycin sulfate, Streptomycin sulfate, and Levofloxacin hydrochloride) in PBS. As seen from Fig. S4, the current responses of the biosensor corresponding to the addition of 10 μM Kanamycin sulfate, 10 μM Streptomycin sulfate, and 10 μM Levofloxacin hydrochloride into PBS are much smaller than the response corresponding to the addition of 10 μM penicillin G and ampicillin sodium salt. These results indicate the good selectivity of the sensor for β-lactam antibiotic detection. In addition, penicillin G and ampicillin sodium salt all belong to β-lactam antibiotic, and responses for these two kinds of β-lactam antibiotic are similar.

4. Conclusions

In summary, this work describes an ultralow detection limit and facile enzymic penicillin biosensor with layer-by-layer (LbL) films of SGN-hematein/ILs/penicillinase. Experimental results suggest that the

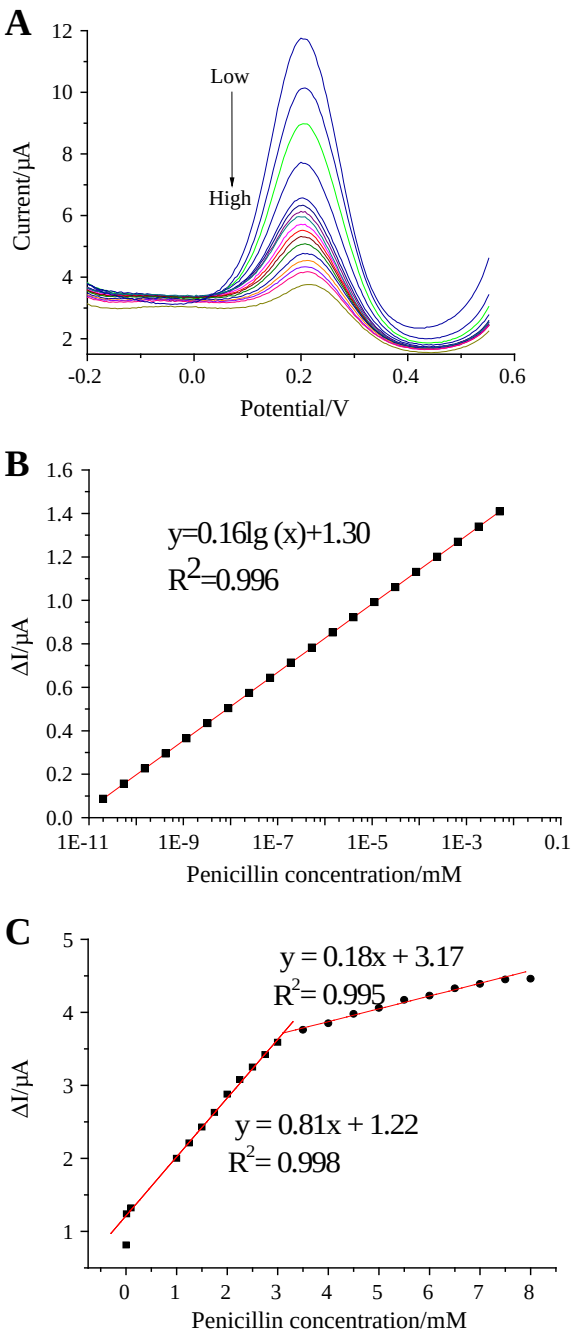

Fig. 7. (A) Differential pulse voltammetric response (DPV) of the SGN-hematein/ILs/penicillinase biosensor with concentration of penicillin G in 20 mL 1 mM pH 6.8 PBS. Calibration curves of background subtracted peak current of DPV at SGN-hematein/ILs/penicillinase versus (B) the low concentration portion of penicillin G in a semi-log format and (C) the high concentration portion of penicillin G in two linear relation curves.

Table 1
Comparison of analytical parameters of various analytical methods for the determination of penicillin G.

Analytical methods	Liner range	Detection limit (nM)	Ref.
LAPS	0.5×10^{-3}–5.0×1.0^{-3} M	–	[12]
CTTPS	0.01–25 mM	1×10^{4}	[13]
Silicon-based sensors	5.0 μM–25 mM	–	[15]
ZnO based biosensor	100 μM–100 mM	–	[27]
MWCNT based biosensor	5.0 nM–2.7 mM	50	[1]
SGN based biosensor	1.25×10^{-13}–7.5×10^{-3} M	1	This work

biosensor displayed excellent performance for penicillin in PBS with three linear relations from 1.25×10^{-13} M to 7.5×10^{-3} M and a relatively low detection limit of 10^{-13} M (0.04 ppt). Moreover, the as-prepared biosensor also exhibited good specificity, high sensitive, acceptable reproducibility and stability. The highlight of this study is to successfully prepare single-graphene nanosheets which have extraordinary electron transport property and high special surface area. Meanwhile, the method adequately utilizes the advantage of ILs based on its film-forming and high ionic conductivity, providing a suitable microenvironment for the immobilized penicillinase, and retaining the biological activity and favorable orientation of penicillinase. So the mixture or combining SGNs and ILs could not only be suitable for the immobilization of penicillinase, but also have potential applications in the fabrication of other enzyme-based biosensor.

Acknowledgments

The authors gratefully acknowledge the financial support from Project for International S & T Cooperation of China (2012DFM30040), the National Science Fund of China (NSFC) (21201035, 61201397), and Fujian Department of Science and Technology (2012J01204).

Appendix A. Supplementary data

Supplementary data to this article can be found online at http://dx.doi.org/10.1016/j.msec.2014.02.012.

References

[1] B. Chen, M. Ma, X. Su, Anal. Chim. Acta. 674 (2010) 89–95.
[2] D. Li, M. Yang, J. Hu, Y. Zhang, H. Chang, F. Jin, Water Res. 42 (2008) 307–317.
[3] M.H. Abouzar, A. Poghossian, J.R. Siqueira Jr., O.N. Oliveira Jr., W. Moritz, M.J. Schöning, Phys. Status Solidi A 207 (2010) 884–890.
[4] M.H. Movassagh, Annu. Biol. Res. 2 (2011) 95–98.
[5] S.M. Santos, M. Henriques, A.C. Duarte, V.I. Esteves, Talanta 71 (2007) 731–737.
[6] R.V. Oliveira, C. Angela, Talanta 70 (2007) 1233–1238.
[7] H.D. Ruyck, H.D. Ridder, Rapid Commun. Mass Spectrom. 21 (2007) 1511–1520.
[8] E. Benito-Peña, J.L. Urraca, M.C. Moreno-Bondi, J. Pharm. Biomed. Anal. 49 (2009) 289–294.
[9] P. Cliquet, B.M. Goddeeris, L. Okermanc, E. Cox, Food Agric. Immunol. 18 (2007) 237–252.
[10] Y. Zhang, Y.M. Jiang, S. Wang, J. Agri, Food Chem. 58 (2010) 8171–8175.
[11] S. Dawana, P. Kanatharanaa, B. Wongkittisuksa, W. Limbut, A. Numnuam, C. Limsakul, P. Thavarungkul, Anal. Chim. Acta. 699 (2011) 232–241.
[12] J.R. Siqueira Jr., C.F. Werner, M. Bäcker, A. Poghossian, V. Zucolotto, O.N. Oliveira Jr., M.J. Schöning, J. Phys. Chem. C 113 (2009) 14765–14770.
[13] S.R. Lee, M.M. Rahman, K. Sawada, M. Ishida, Biosens. Bioelectron. 24 (2009) 1877–1882.
[14] A. Poghossian, T. Yoshinobu, A. Simonis, H. Ecken, H. Lüth, M.J. Schöning, Sens. Actuators B 78 (2001) 237–242.
[15] J.R. Siqueira Jr., M.H. Abouzar, A. Poghossianb, V. Zucolotto, O.N. Oliveira Jr., M.J. Schöning, Biosens. Bioelectron. 25 (2009) 497–501.
[16] B. Chen, M. Ma, X.L. Su, Anal. Chim. Acta. 674 (2010) 89–95.
[17] E.Y. Choi, T.H. Han, J. Hong, J.E. Kim, S.H. Lee, H.W. Kim, S.O. Kim, J. Mater. Chem. 20 (2010) 1907–1912.
[18] Y. Wang, Y. Shao, D.W. Matson, J. Li, Y. Lin, ACS Nano 4 (2010) 1790–1798.
[19] J. Li, C. Liu, C. Cheng, Electrochim. Acta 56 (2011) 2712–2716.
[20] M. Pumera, A. Ambrosi, A. Bonanni, E.L.K. Chng, H.L. Poh, Anal. Chem. 29 (2010) 954–965.
[21] K. Liu, J. Zhang, G. Yang, C. Wang, J. Zhu, Electrochem. Commun. 12 (2010) 402–405.
[22] C. Shan, H. Yang, D. Han, Q. Zhang, A. Ivaska, L. Niu, Biosens. Bioelectron. 25 (2010) 1504–1508.
[23] S. Alwarappan, A. Erdem, C. Liu, C.Z. Li, J. Phys. Chem. C 113 (2009) 8853–8857.
[24] C. Shan, H. Yang, J. Song, D. Han, A. Ivaska, L. Niu, Anal. Chem. 81 (2009) 2378–2382.
[25] C. Fu, Y. Kuang, Z. Huang, X. Wang, N. Du, J. Chen, H. Zhou, Chem. Phys. Lett. 499 (2010) 250–253.
[26] C.X. Guo, Z.S. Lu, Y. Lei, C.M. Li, Electrochem. Commun. 12 (2010) 1237–1240.
[27] N. Maleki, A. Safavi, F. Sedaghati, F. Tajabadi, Anal. Biochem. 369 (2007) 149–153.
[28] S. Guo, D. Wen, Y. Zhai, S. Dong, E. Wang, Biosens. Bioelectron. 26 (2011) 3475–3481.
[29] M. Du, T. Yang, S. Ma, C. Zhao, K. Jiao, Anal. Chim. Acta. 690 (2011) 169–174.
[30] Q. Zhang, S. Wu, L. Zhang, J. Lu, F. Verproot, Y. Liu, Z. Xing, J. Li, X. Song, Biosens. Bioelectron. 26 (2011) 2632–2637.
[31] M. Feng, R. Sun, H. Zhan, Y. Chen, Nanotechnology 21 (2010) (075601–1–7).
[32] W.S. Hummers Jr., R.E. Offeman, J. Am. Chem. Soc. 6 (1958) 1339.
[33] A.P. Chiriac, L.E. Nita, I. Nemtu, C.M. Popescu, A. Ioanid, G.E. Ioanid, Rom. J. Physiol. 50 (2005) 1119–1126.

[34] X. Tong, H. Wang, G. Wang, L. Wan, Z. Ren, J. Bai, J. Bai, J. Solid State Chem. 184 (2011) 982–989.
[35] J.I. Paredes, S. Villar-Rodil, A. Martínez-Alonso, J.M.D. Tascón, Langmuir 24 (2008) 10560–10564.
[36] T.Y. Kim, H.W. Lee, J.E. Kim, K.S. Suh, ACS Nano 4 (2010) 1612–1618.
[37] D. Li, M.B. Muller, S. Gilje, R.B. Kaner, G.G. Wallace, Nat. Nanotechnol. 3 (2008) 101–105.
[38] F. Giannazzo, S. Sonde, V. Raineri, E. Rimini, Nano Lett. 9 (2009) 23–29.
[39] G.A.M. Mersal, H.A. Arida, Int. J. Electrochem. Sci. 6 (2011) 1116–1126.
[40] F.H. Wu, Z.C. Hu, L.W. Wang, J.J. Xu, Y.Z. Xian, Y. Tian, L.T. Jin, Electrochem. Commun. 10 (2008) 630–634.